Journal of Electroanalytical Chemistry 820 (2018) 67–73

Contents lists available at ScienceDirect

Journal of Electroanalytical Chemistry

journal homepage: www.elsevier.com/locate/jelechem

Soret coefficient of trace ions determined with electrochemical impedance spectroscopy in a thin cell. Theory and measurement

Miikka Jokinen[a], José A. Manzanares[a,b], Lasse Murtomäki[a,*]

[a] Department of Chemistry, School of Chemical Engineering, Aalto University, P.O. Box 16100, FI-00076 Aalto, Finland
[b] Department of Thermodynamics, Faculty of Physics, University of Valencia, E-46100 Burjassot, Spain

ARTICLE INFO

Keywords:
Thermodiffusion
Impedance
Soret effect
Thin film cell

ABSTRACT

The tendency of a substance to migrate due to a temperature gradient is known as thermodiffusion or the Soret effect. We believe that this is the first work that describes the study of the Soret effect using electrochemical impedance spectroscopy in a non-isothermal thin cell, and shows how the Soret coefficient can be determined from these measurements. The effect of a temperature gradient in a thin cell is analyzed, both theoretically and experimentally. Our theoretical modeling of the system predicts the effect of key parameters to the impedance spectra. Experimentally we determine the Soret coefficient of the redox couple $Fe(CN)_6^{4-}/Fe(CN)_6^{3-}$ in an aqueous KCl solution. It is found that the Soret coefficient decreases with increasing ionic strength in the studied concentration range.

1. Introduction

Transport of a solute due to a temperature gradient is known as thermodiffusion. The Soret effect builds up an equilibrium concentration distribution in which diffusion and thermodiffusion contributions to the flux density of a solute cancel each other. The Soret coefficient $\sigma_{T,i} = -(\partial \ln c_i/\partial T)_{j_i=0}$ of species i describes its equilibrium concentration gradient in the presence of a temperature gradient [1]. The Soret effect affects, for example, mass transport at heated microelectrodes [2], and it can be used to analyze the thermoelectric efficiency of different electrolytes [3]. It can also provide information on the structure of electrolyte solutions [4], or be applied as a tool in biomolecule analytics [5,6] and in polymer separation and purification processes [7,8]. Furthermore, this effect may have played an important role in the origin of life [9].

Accurate measurements of the Soret coefficient are difficult, mainly due to the long measurement times required for the concentration difference to develop, and convective mixing which easily disturbs the measurement. For concentrated electrolyte solutions [10], and non-electrolyte solutions [11], the Soret coefficient has been determined optically by measuring changes in the refractive index along a temperature gradient, and relating them to the concentration changes. In dilute electrolyte solutions, however, the method becomes unsatisfactory [2], and other methods should be used. These include the so-called conductivity method, where changes in conductivity of a non-isothermal cell correspond to changes in concentrations [12–14], and the thermoelectric power method, where the initial and steady-state electromotive force of a non-isothermal cell is linked to the heat of transport of the electrolyte [15]. Results achieved with these methods suggest that the Soret coefficients of electrolytes depend strongly on the concentration [15] and size of the transported particles [4]. It has been also suggested that a supporting electrolyte can significantly enhance thermodiffusion in dilute solutions [8], but the hypothesis was not experimentally confirmed due to the lack of a suitable measurement technique. Later, the presence of the Soret phenomenon for a trace ion in a supporting electrolyte was observed in a study of mass transport at hot microelectrodes [2], but due to the complicated nature of the experimental setup, the effect could only be studied qualitatively.

Here, we show how thermodiffusion of a trace ion can be studied with electrochemical impedance spectroscopy (EIS) in a non-isothermal thin cell. Impedance spectroscopy has been previously utilized in non-isothermal systems only by the periodical modulation of the temperature of the working electrode, a method known as thermoelectrochemical impedance [16]. However, the determination of the Soret coefficient using this approach is problematic because the temperature gradient can be poorly defined. Here we show that by applying a temperature gradient between the working electrode (WE) and the counter electrode (CE) in a thin cell, it is possible to study its effect on the mass transport and to measure the ionic Soret coefficient of the reacting trace ions.

* Corresponding author.
E-mail address: lasse.murtomaki@aalto.fi (L. Murtomäki).

https://doi.org/10.1016/j.jelechem.2018.04.054
Received 23 February 2018; Received in revised form 18 April 2018; Accepted 24 April 2018
Available online 27 April 2018

2. Theory

We consider one-dimensional transport of a redox species in a thin cell, with the WE at $x = 0$ and the CE at $x = h$. In excess of a supporting electrolyte, migration is negligible and the molar flux density of species i (i = O, R) is [17]

$$-j_i = D_i\left(c_i\sigma_{T,i}\frac{\partial T}{\partial x} + \frac{\partial c_i}{\partial x}\right) = \frac{2D_i}{h}\left(\theta_i c_i + \frac{\partial c_i}{\partial \xi}\right) \tag{1}$$

where D_i, c_i and $\sigma_{T,i}$ are the diffusion coefficient, the concentration and the Soret coefficient of species i, and $\theta_i = \sigma_{T,i}\Delta T/2$ with $\Delta T = T(h) - T(0)$. The assumption of temperature independent diffusion coefficients introduces a negligible error when ΔT is moderate [15], especially in the case of constant average temperature in the cell. In the second equality of Eq. (1), a linear temperature distribution has been assumed and the dimensionless spatial coordinate $\xi = 2x/h - 1$ has been introduced. The concentration distribution under Soret equilibrium ($j_i = 0$) is $c_{i,\mathrm{eq}}(\xi) = c^s{}_{i,\mathrm{eq}}\,\mathrm{e}^{-(1+\xi)\theta_i}$, and the surface concentrations at the WE ($\xi = -1$) are

$$c^s_{i,\mathrm{eq}} = c_i{}^{\mathrm{b}}E_{\theta,i}, \tag{2}$$

where $c_i{}^{\mathrm{b}} = (1/2)\int_{-1}{}^{1}c_{i,\mathrm{eq}}\mathrm{d}\xi$ is the average concentration and $E_{\theta,i} = 2\theta_i/(1 - \mathrm{e}^{-2\theta_i})$ is the thermophoretic factor of species i.

The relation between the flux density and the current density $i(t)$ is $j_{\mathrm{O}}|_{\xi=\pm1} = -j_{\mathrm{R}}|_{\xi=\pm1} = i(t)/F$. Electric current perturbs the equilibrium distribution so that

$$c_i(\xi,t) = c_{i,\mathrm{eq}}(\xi) + \delta c_i(\xi,t) \tag{3}$$

$$\pm\frac{i}{2FD_i/h} = \left(\theta_i\delta c_i + \frac{\partial\delta c_i}{\partial\xi}\right)\Bigg|_{\xi=\pm1} \tag{4}$$

where the $+(-)$ sign in the left hand side of Eq. (4) applies to species R (O). The continuity equation $\partial\delta c_i/\partial t = -\partial j_i/\partial x$ can be written as

$$t_{\mathrm{D},i}\frac{\partial\delta c_i}{\partial t} = \theta_i\frac{\partial\delta c_i}{\partial\xi} + \frac{\partial^2\delta c_i}{\partial\xi^2} \tag{5}$$

where $t_{\mathrm{D},i} = h^2/4D_i$. Since $\delta c_i(\xi,0) = 0$, the Laplace transform of Eq. (5) is

$$t_{\mathrm{D},i}s\bar{c}_i = \theta_i\frac{\mathrm{d}\bar{c}_i}{\mathrm{d}\xi} + \frac{\mathrm{d}^2\bar{c}_i}{\mathrm{d}\xi^2} \tag{6}$$

where $\bar{c}_i = \int_0^\infty \delta c_i(\xi,t)\mathrm{e}^{-st}\mathrm{d}t$, and its solution can be presented as

$$\bar{c}_i(\xi) = A_i r_{1,i}\mathrm{e}^{r_{1,i}\xi} - B_i r_{2,i}\mathrm{e}^{-r_{2,i}\xi} \tag{7}$$

where

$$r_{1,i} = \rho_i - \frac{\theta_i}{2},\quad r_{2,i} = r_{1,i} + \theta_i,\quad \rho_i = \left(t_{\mathrm{D},i}s + \frac{\theta_i^2}{4}\right)^{\frac{1}{2}}. \tag{8}$$

Integration of Eq. (5) with respect to ξ and the condition $j_i|_{\xi=-1} = j_i|_{\xi=1}$ imply $(\partial/\partial t)\int_{-1}{}^{1}\delta c_i\mathrm{d}\xi = 0$ and hence $\int_{-1}^{1}\bar{c}_i\mathrm{d}\xi = 0$. Thus, we conclude that $B_i = A_i\sinh r_{1,i}/\sinh r_{2,i}$. Moreover, since $r_{1,i}{}^2 + r_{1,i}\theta_i = r_{2,i}{}^2 - r_{2,i}\theta_i = r_{1,i}r_{2,i} = t_{\mathrm{D},i}s$, Eq. (4) implies that

$$\pm\frac{\bar{i}(s)}{2FD_i/h} = A_i t_{\mathrm{D},i}s\frac{\sinh 2\rho_i}{\sinh r_{2,i}}. \tag{9}$$

Thus, A_i can be solved in terms of the Laplace transform of the current density, $\bar{i}(s)$. Substituting these values of A_i and B_i into Eq. (7), the concentration of species i is

$$\bar{c}_i(\xi) = \pm\frac{\bar{i}(s)}{2FD_i/h}\frac{r_{1,i}\mathrm{e}^{r_{1,i}\xi}\sinh r_{2,i} - r_{2,i}\mathrm{e}^{-r_{2,i}\xi}\sinh r_{1,i}}{t_{\mathrm{D},i}s\,\sinh 2\rho_i} \tag{10}$$

and its value at the WE ($\xi = -1$) is

$$\bar{c}^s_i = \pm\frac{\bar{i}(s)}{2FD_i/h}\frac{1}{t_{\mathrm{D},i}s}\left(-\rho_i\tanh\rho_i - \frac{\theta_i}{2} + \rho_i\frac{\mathrm{e}^{\theta_i} - 1}{\sinh 2\rho_i}\right). \tag{11}$$

The net current equals the difference in the rates of the oxidation and reduction reactions

$$\frac{i}{F} = k_{\mathrm{ox}}c^s_{\mathrm{R}} - k_{\mathrm{red}}c^s_{\mathrm{O}} = k_{\mathrm{ox,eq}}\mathrm{e}^{\alpha f\eta}c^s_{\mathrm{R}} - k_{\mathrm{red,eq}}\mathrm{e}^{(\alpha-1)f\eta}c^s_{\mathrm{O}} \tag{12}$$

where $\eta = E - E_{\mathrm{eq}}$ is the overpotential, α is the transfer coefficient, $k_{\mathrm{ox,eq}} = k^0\exp[\alpha f(E_{\mathrm{eq}} - E^{0\prime})]$ and $k_{\mathrm{red,eq}} = k^0\exp[(\alpha-1)f(E_{\mathrm{eq}} - E^{0\prime})]$ are the equilibrium rate constants, k^0 is the standard rate constant, and $f = F/RT(0)$. Note that the temperature $T(0) = \overline{T} - \Delta T/2$ of the WE differs from the average temperature $\overline{T}$. Since the Soret effect changes the equilibrium surface concentrations, Eq. (2), the Nernst equilibrium potential of the WE is

$$E_{\mathrm{eq}} = E^{0\prime} + \frac{1}{f}\ln\left(\frac{c^{\mathrm{b}}_{\mathrm{O}}}{c^{\mathrm{b}}_{\mathrm{R}}}\frac{E_{\theta,\mathrm{O}}}{E_{\theta,\mathrm{R}}}\right). \tag{13}$$

At equilibrium ($i = 0$, $\eta = 0$), the oxidation and reduction reactions occur at the same rate, which defines the exchange current density

$$i_0 = Fk_{\mathrm{ox,eq}}c^s_{\mathrm{R,eq}} = i_0{}^{\mathrm{b}}(E_{\theta,\mathrm{O}})^{\alpha}(E_{\theta,\mathrm{R}})^{1-\alpha} \tag{14}$$

where $i_0{}^{\mathrm{b}} = Fk^0(c_{\mathrm{O}}{}^{\mathrm{b}})^{\alpha}(c_{\mathrm{R}}{}^{\mathrm{b}})^{1-\alpha}$.

Since Eq. (11) shows that $c^s{}_i - c^s{}_{i,\mathrm{eq}}$ is proportional to the current density, the linearized form of the current-overpotential equation is

$$\frac{i}{i_0} = \frac{c^s_{\mathrm{R}}}{c^s_{\mathrm{R,eq}}}\mathrm{e}^{\alpha f\eta} - \frac{c^s_{\mathrm{O}}}{c^s_{\mathrm{O,eq}}}\mathrm{e}^{(\alpha-1)f\eta} \approx \frac{c^s_{\mathrm{R}} - c^s_{\mathrm{R,eq}}}{c^s_{\mathrm{R,eq}}} - \frac{c^s_{\mathrm{O}} - c^s_{\mathrm{O,eq}}}{c^s_{\mathrm{O,eq}}} + f\eta \tag{15}$$

and its Laplace transform is

$$\frac{\bar{i}}{i_0} \approx \frac{\bar{c}^s_{\mathrm{R}}}{c^s_{\mathrm{R,eq}}} - \frac{\bar{c}^s_{\mathrm{O}}}{c^s_{\mathrm{O,eq}}} + f\bar{\eta} \tag{16}$$

Using Eq. (11) the electrochemical impedance $Z = \bar{\eta}/A\bar{i}$ is

$$\begin{aligned} Z(s) = {} & R_{\mathrm{ct}} + \\ & R^s_{\mathrm{O,eq}}\left(\rho_{\mathrm{O}}\tanh\rho_{\mathrm{O}} + \tfrac{\theta_{\mathrm{O}}}{2} - \rho_{\mathrm{O}}\tfrac{\mathrm{e}^{\theta_{\mathrm{O}}}-1}{\sinh 2\rho_{\mathrm{O}}}\right)\tfrac{1}{t_{\mathrm{D,O}}s} + \\ & R^s_{\mathrm{R,eq}}\left(\rho_{\mathrm{R}}\tanh\rho_{\mathrm{R}} + \tfrac{\theta_{\mathrm{R}}}{2} - \rho_{\mathrm{R}}\tfrac{\mathrm{e}^{\theta_{\mathrm{R}}}-1}{\sinh 2\rho_{\mathrm{R}}}\right)\tfrac{1}{t_{\mathrm{D,R}}s} \end{aligned} \tag{17}$$

where $R_{\mathrm{ct}} = 1/(fAi_0) = R(\overline{T} - \Delta T/2)/(FAi_0)$ is the charge-transfer resistance, A is the WE area, and $R^s{}_{i,\mathrm{eq}} = RT(0)h/(2F^2AD_ic^s{}_{i,\mathrm{eq}})$ is the ohmic resistance associated to species i. The zero-frequency ($t_{\mathrm{D},i}s \to 0$) limit of Eq. (17) is

$$Z(\omega \to 0) = R_{\mathrm{ct}} + R^s_{\mathrm{O,eq}}[1 + \mathrm{L}(\theta_{\mathrm{O}})] + R^s_{\mathrm{R,eq}}[1 + \mathrm{L}(\theta_{\mathrm{R}})] \tag{18}$$

where $\mathrm{L}(x) = \coth(x) - 1/x$ is the Langevin function. For small temperature gradients ($\theta_i \ll 1$), the impedance reduces to

$$\begin{aligned} \left(1 - \frac{\Delta T}{2\overline{T}}\right)^{-1}Z(s) \approx {} & R^{\mathrm{b}}_{\mathrm{ct}}[1 - \alpha\theta_{\mathrm{O}} - (1-\alpha)\theta_{\mathrm{R}}] \\ & + R^{\mathrm{b}}_{\mathrm{O}}\frac{\tanh\sqrt{t_{\mathrm{D,O}}s} - \mathrm{L}(2\sqrt{t_{\mathrm{D,O}}s})\theta_{\mathrm{O}}}{\sqrt{t_{\mathrm{D,O}}s}} \\ & + R^{\mathrm{b}}_{\mathrm{R}}\frac{\tanh\sqrt{t_{\mathrm{D,R}}s} - \mathrm{L}(2\sqrt{t_{\mathrm{D,R}}s})\theta_{\mathrm{R}}}{\sqrt{t_{\mathrm{D,R}}s}} \end{aligned} \tag{19}$$

where $R^{\mathrm{b}}_{\mathrm{ct}} = R\overline{T}/(FAi_0{}^{\mathrm{b}})$ and we have used $c^s{}_{\mathrm{eq},i}/c_i{}^{\mathrm{b}} = E_{\theta,i} \approx 1 + \theta_i$ and $T(0) = \overline{T} - \Delta T/2$.

In the isothermal case ($\theta_i = 0$, $\rho_i = \sqrt{t_{\mathrm{D},i}s}$) the thermodiffusion impedance includes the tanh-type elements characterizing diffusion in a thin-layer cell [18]

$$Z(\omega) = \lim_{s\to j\omega}Z(s) = R^{\mathrm{b}}_{\mathrm{ct}} + R^{\mathrm{b}}_{\mathrm{O}}\frac{\tanh\sqrt{j\omega t_{\mathrm{D,O}}}}{\sqrt{j\omega t_{\mathrm{D,O}}}} + R^{\mathrm{b}}_{\mathrm{R}}\frac{\tanh\sqrt{j\omega t_{\mathrm{D,R}}}}{\sqrt{j\omega t_{\mathrm{D,R}}}} \tag{20}$$

which at zero frequency reduces to $Z(\omega \to 0, \theta_i \to 0) = R_{\mathrm{ct}}{}^{\mathrm{b}} + R_{\mathrm{O}}{}^{\mathrm{b}} + R_{\mathrm{R}}{}^{\mathrm{b}}$ where $R^{\mathrm{b}}_i = R\overline{T}h/(2F^2AD_ic_i{}^{\mathrm{b}})$. In the non-isothermal case,

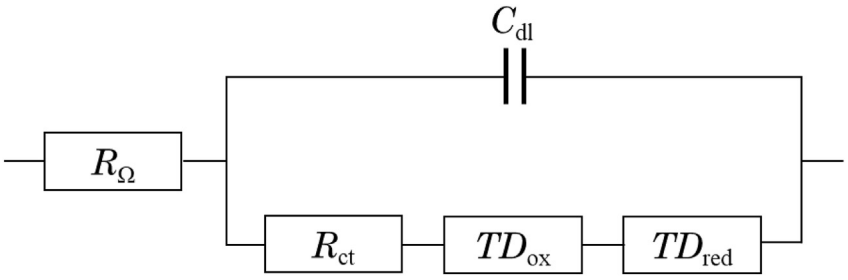

Fig. 1. The thermodiffusion impedance circuit. R_Ω is the ohmic resistance, C_{dl} the double layer capacitance, R_{ct} the charge transfer resistance and *TD* the thermodiffusion element.

from Eq. (18) or (19), the zero-frequency limit of the impedance is

$$Z(\omega \to 0) \approx \left(1 - \frac{\Delta T}{2\overline{T}}\right)\left\{R_{ct}^{b}[1 - \alpha\vartheta_O + (\alpha - 1)\vartheta_R] + R_O^{b}\left(1 - \frac{\sigma_{T,O}\Delta T}{3}\right) + R_R^{b}\left(1 - \frac{\sigma_{T,R}\Delta T}{3}\right)\right\}. \quad (21)$$

Eq. (21) shows that an increase in the temperature difference (i.e. an increase of the temperature of the CE with respect to that of the WE) leads to a decrease in the low-frequency resistance. From the limit $\omega \to 0$, and measurements with different concentration ratios ${c_O}^b/{c_R}^b$, it seems possible to determine the individual Soret coefficients.

The model derived here predicts that two effects can be observed. The first effect of the temperature gradient is the change in the equilibrium concentrations at the electrode, Eq. (2), which has a small effect on the observed equilibrium potential and exchange current density, i.e. on the transfer kinetics. The second effect stems from thermodiffusion, i.e. mass transport, which is overlapped with "ordinary" diffusion and taken into account in the transport element. The equivalent circuit of the impedance in Eq. (17) is shown in Fig. 1. In some cases, it might be beneficial to analyze the impedance at the limit $\omega \to 0$, by extrapolating the experimental data towards the real impedance axis.

3. Experimental

The measurements were done in a custom made thin cell consisting of two (PVC) polymer blocks (Fig. 2). The bottom block had flow channels carved onto it, so that electrolyte could be pumped through the cell. The bottom block also had an aperture for the working electrode, a platinum cylinder (5 mm in diameter) connected to a copper rod by a gold solder. The rod ran through the bottom block before being connected to a larger copper block, which acted as a heat sink. The WE was aligned with the level of the flow channels, creating an even inner surface in the cell. The top block was sealed to the bottom with a thin rubber gasket. Aligned with the WE was the counter electrode: an identical platinum cylinder (5 mm in diameter) soldered to a copper screw, which ran through the top block. The screw acted as a heat source: a few cm of it stuck outside the cell, and resistive wire was wrapped around it. The screw could be turned, enabling the control of the distance between the two electrodes to a certain extent. A 260 µm thick glass fiber separator (GF/A, Whatman, UK) was placed between the electrodes to prevent short circuiting, and a thin Ag/AgCl electrode was placed near the two platinum electrodes, before the cell was closed with screws. The joints between the copper parts and the plastic blocks were sealed with two-component silicon sealant. The temperatures of the platinum cylinders were measured at a distance of 1 mm from the surface with two K-type thermocouples, placed in holes drilled through the copper rod and screw and into the platinum cylinders. Because the thermal conductivity of platinum in 298 K is much larger than of water ($71.6\,W\,m^{-1}\,K^{-1}$ and $0.61\,W\,m^{-1}\,K^{-1}$, respectively [19]), the measured temperatures were consider to be equal to those at the electrode surfaces: if the distance between the two electrodes is 0.26 mm and filled with water, approximately 94% of the measured temperature difference at 1 mm distance from both surfaces resides in the water. The temperature of the copper block in contact with the WE (Cu′) was controlled with a Peltier-element (MCPK2-19808 AC-S, Multicomp, USA), and the temperature of the other copper block (Cu″) was controlled with a resistive wire and a power source (SPD3303C, Siglent Technologies, China).

The electrodes were heated to the desired temperatures (± 0.5 °C) keeping the average temperature of the cell constant at $\overline{T} = 298$ K. A solution of the desired concentrations of $K_4[Fe(CN)_6]$ (99%, from trihydrate salt, Sigma-Aldrich) and $K_3[Fe(CN)_6]$ (p.a., Merck) in 0.5 mol/L KCl (Ph. Eur., VWR) supporting electrolyte was prepared in ion-exchanged water and purged with humidified N_2 gas to remove oxygen. The ferro/ferricyanide solution was then pumped through the cell with a peristaltic pump (IPN, Ismatec, Germany). The impedance was measured at the open-circuit potential in the frequency range of 100 kHz − 1 mHz. The impedance data was fitted to the model circuit

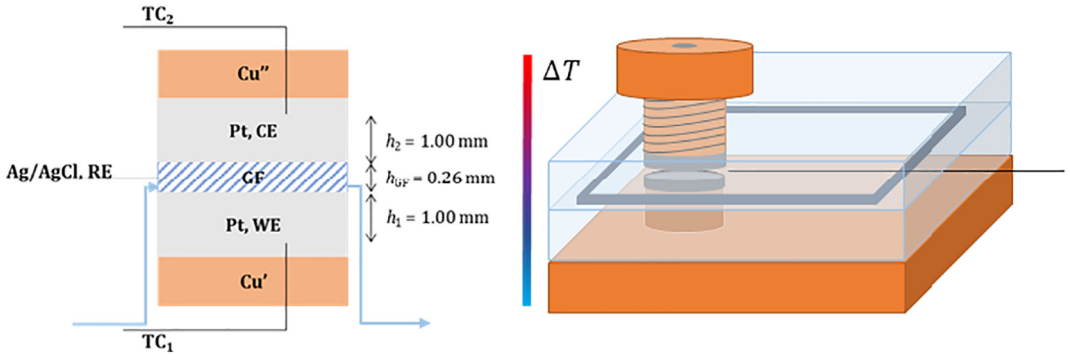

Fig. 2. Left: Schematic of the measurement setup and the cell diagram. The WE (lower block) and the CE are platinum, and the reference electrode is a thin Ag/AgCl wire. A 260 µm glass fiber separator is clamped between the WE and the CE. Two copper blocks, Cu′ and Cu″, are used as the heat sink and source, respectively. The temperatures of the electrodes are measured with two K-type thermocouples at 1 mm distance from the electrode surfaces and controlled with a Peltier element and a heating wire. The temperature gradient runs vertically through the cell. The colder side is at the bottom to reduce thermal convection. Right: 3D sketch of the cell.

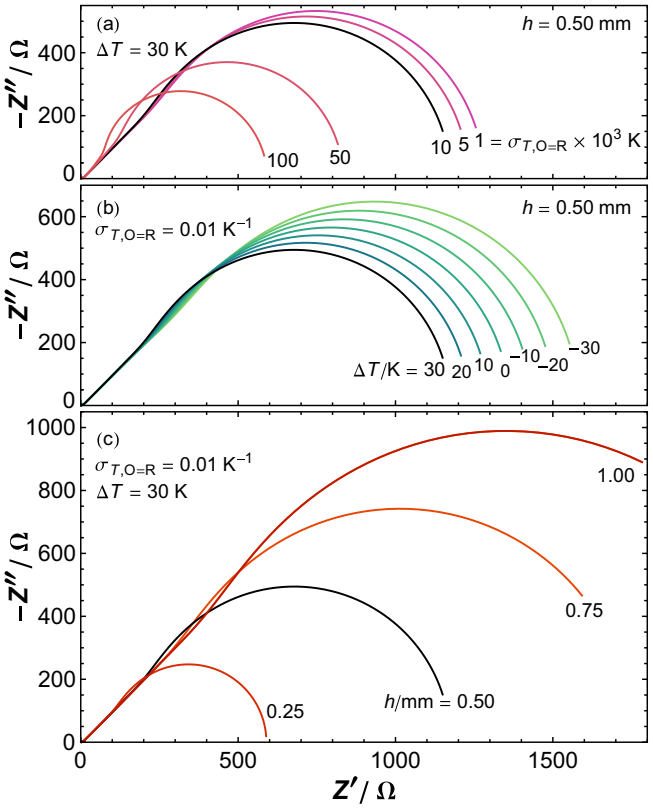

Fig. 3. Simulated thermodiffusion impedance (f = 100 kHz − 1 mHz) corresponding to the bulk concentrations $c_O^b = c_R^b$ = 5 mmol/L, electrode diameter d = 5 mm, $\overline{T}$ = 298 K, R_Ω = 1 Ω, C_{dl} = 5 μF, R_{ct} = 5Ω, and $D_O = D_R = 10^{-5}$ cm^2/s. The impedance spectrum is sensitive to the Soret coefficient (panel (a)) using moderate temperature gradients (panel (b)), but it is also very sensitive to cell parameters like the cell thickness h (panel (c)). The simulation with $\sigma_{T,O} = \sigma_{T,R}$ = 0.01 K^{-1}, ΔT = 30 K and h = 500 μm is shown in black in the three panels to help their comparison.

using the Matlab impedance fitting code Zfit (v.1.2) by Jean-Luc Dellis [20].

4. Results and discussion

4.1. Simulations

The impedance of the equivalent circuit with thermodiffusion elements (Fig. 1) exhibits two semicircles: the first one is due to the charge transfer resistance in parallel with the electrode capacitance, and the second one due to mass transport in a confined space. Fig. 3 shows the effect of varying $\sigma_{T,O} = \sigma_{T,R}$, ΔT and h on the impedance calculated from Eq. (17). The bulk concentrations $c_O^b = c_R^b$ = 5 mmol/L, electrode diameter d = 5 mm, average temperature of the system $\overline{T}$ = 298 K, solution resistance R_Ω = 1 Ω, double layer capacitance C_{dl} = 5 μF, charge transfer resistance R_{ct} = 5 Ω, and diffusion coefficients $D_O = D_R = 10^{-5}$ cm^2/s are kept constant. Keeping ΔT = 30 K constant and increasing the Soret coefficient from $\sigma_{T,O} = \sigma_{T,R}$ = 0.001 K^{-1} to 0.005 K^{-1} results in a small but clear decrease in the low-frequency impedance (Fig. 3a). The larger the Soret coefficient, the smaller the low-frequency impedance is, as the Soret effect enriches the ions at the colder WE surface. Varying the temperature difference from −30 K to +30 K results in impedance curves (Fig. 3b) significantly different from that of an isothermal cell, Eq. (20). Changing the cell thickness h has a dramatic effect on the size of the second semicircle: the maximum value of $-Z''$ increases linearly with h (Fig. 3c). Note that the lowest frequency considered, f = 1 mHz, satisfies the limit $f \ll D_i/h^2$ (which corresponds to $t_{D,i}s \ll 1$) when h = 0.25 mm but not when

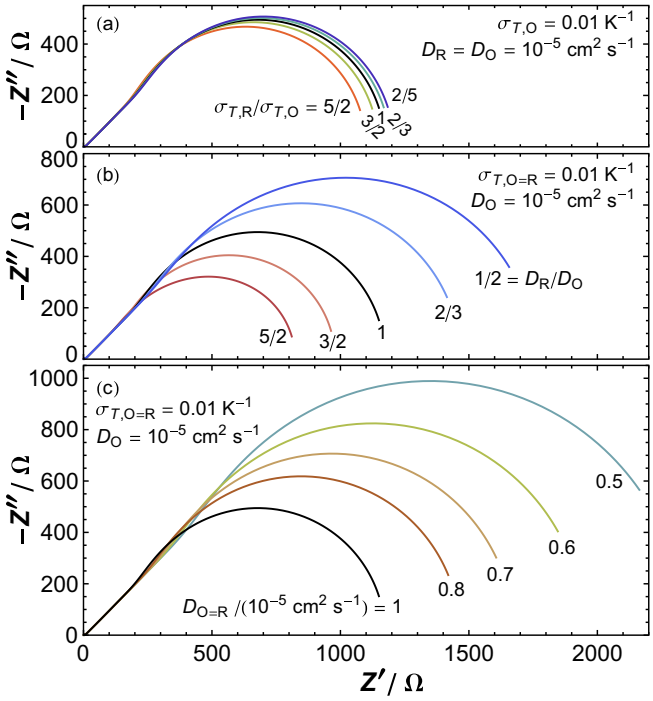

Fig. 4. Simulated impedance (f = 100 kHz − 1 mHz) with ΔT = 30 K and h = 500 μm. The values of the parameters $c_O^b = c_R^b$, d, $\overline{T}$, R_Ω, C_{dl}, and R_{ct} are the same as in Fig. 3. The impedance is weakly sensitive to the ratio of Soret coefficients of the reduced and oxidized species (panel (a)) and it is quite sensitive to the ratio of their diffusion coefficients (panel (b)) and to the values of the diffusion coefficients when they are the same for both species (panel (c)). The simulation with $\sigma_{T,O} = \sigma_{T,R}$ = 0.01 K^{-1} and $D_O = D_R = 10^{-5}$ cm^2/s is shown in black in the three panels.

h = 1.0 mm. The key role of the cell thickness on the frequency dependence of the impedance can also be analyzed using the Bode plots in Fig. SI.1 of the Supporting Information.

The model takes into account that the diffusion and Soret coefficients of the oxidized and reduced species might be different. Fig. 4 shows how the impedance changes when these coefficients are altered while keeping ΔT = 30 K, h = 500 μm, and c_O^b, c_R^b, d, $\overline{T}$, R_Ω, C_{dl}, and R_{ct} as in Fig. 3. Fig. 4a shows the case where the reduced and oxidized species have the same diffusion coefficients and different Soret coefficients. It is observed that the impedance is not very sensitive to the difference in the Soret coefficients, although it is sensitive to their values (Fig. 3a). Fig. 4b shows the case where the reduced and oxidized species have the same Soret coefficients and different diffusion coefficients. The diffusion coefficient for the oxidized species is kept constant at $D_O = 10^{-5}$ cm^2/s, and the value for the reduced species is changed. As D_R increases, the transport of the reduced species is enhanced and the impedance decreases, and vice versa. In Fig. 4c, the two species have the same diffusion coefficient, but its value is decreased from $D_O = D_R = 10^{-5}$ cm^2/s while the Soret coefficient is kept constant at $\sigma_{T,O} = \sigma_{T,R}$ = 0.01 K^{-1}. The comparison of Figs. 4c and 3a highlights the difference in sensitivity towards the value of the diffusion coefficient and the Soret coefficient. From the case with $D_O = D_R = 10^{-5}$ cm^2/s and $\sigma_{T,O} = \sigma_{T,R}$ = 0.01 K^{-1} (shown in black in the three panels of Figs. 3 and 4 to help their comparison), a 20% decrease in the diffusion coefficient to $D_O = D_R = 0.8 \times 10^{-5}$ cm^2/s has almost the same effect as reversing the direction of the temperature gradient from 30 K to −30 K (compare to Fig. 3b).

4.2. Experimental results

The theoretical model predicts the shape of the impedance spectra

as a large semicircle, which approaches the real axis at low frequencies. For the typical case of positive Soret coefficient $\sigma_{T,i}$, a positive temperature difference, $T_{WE} < T_{CE}$, enhances the mass transport to the working electrode. This should manifest itself as a decrease in the size of the low-frequency semicircle. The measurements confirm this prediction.

The simulations show that the impedance is very sensitive to h, D_O, and D_R (Figs. 3c and 4c), and not so sensitive to the Soret coefficient or the temperature difference (Figs. 3a, b and 4a). The cell thickness h and the diffusion coefficients D_i appear in the expression of the impedance through the diffusional times $t_{D,i} = h^2/4D_i$. Hence, the values of h and D_i cannot and need not be fitted separately. The ratio of the diffusion coefficients of the ferrocyanide/ferricyanide redox couple is particularly important (Fig. 4b). The usual assumption of $D_O = D_R$ is likely to cause significant error in the analysis; on the contrary, the effect of O and R having different Soret coefficient is negligible (Fig. 4a). The ratio D_R/D_O can be approximated by its value at infinite dilution and 298 K, the average temperature in the cell. Since $D_O = 0.9 \times 10^{-5}$ cm^2/s and $D_R = 0.73 \times 10^{-5}$ cm^2/s at infinite dilution [21], we have fixed $D_R/D_O = 0.81$. Then, in order to determine the value of the Soret coefficient with a meaningful precision, only the diffusional times $t_{D,R}$ have to be determined accurately; $t_{D,O}$ can be calculated from $t_{D,R}$ and D_R/D_O.

For every concentration, the impedance was measured with and without temperature gradient, at $\overline{T} = 298$ K. The isothermal measurement was used to determine some cell parameters, which were then used in the analysis of the non-isothermal impedance, thus decreasing the number of fitting parameters in the latter. The fitting procedure is now explained in detail. First, the ohmic resistance was determined and fixed as the point where the high frequency impedance should intercept the real axis. The concentrations were taken as their targeted values. Initial values for the parameters were obtained from an educated guess: the effective surface area A was estimated as geometric area and $t_{D,R}$ was estimated as 54.8 s from $D_R \approx 0.73 \times 10^{-5}$ cm^2/s and an estimated thickness h of 400 μm. Then, the high-frequency data (21 points, 100 kHz–10 Hz) were fitted to the isothermal model, which gave values of the kinetic parameters: the charge transfer resistance R_{ct} and the parameters of the constant phase element, $1/Z_{CPE} = (j\omega)^n Q$ where $n \leq 1$. Subsequently, the values of the kinetic parameters were locked, and A and $t_{D,R}$ were used as fitting parameters for the whole frequency range, yielding an adequate fit for both high and low frequencies. The separate fitting of the high frequency range was necessary to ensure that physically meaningful values were obtained; the low frequency data with the larger modulus gets a larger weight in the fitting process. Without the above mentioned procedure, the frequency exponent of the CPE, n, tended to set between 0 and 0.5, which clearly does not represent reality at high frequencies, although it showed a nice fit to the experimental impedance at low frequencies.

Fig. 5 shows experimental results for $c_O^b = c_R^b = 10$ mmol/L, where (a) shows the isothermal measurement and (b) the measurement with a temperature gradient. The circles represent the experimental points and the lines are fit results. The inset in Fig. 5a shows the result from the high frequency fit. The frequency dependence of the impedance can also be analyzed using the Bode plots in Fig. SI.2 of the Supporting Information. The ohmic resistance is 0.50 Ω, and the high frequency semicircle corresponds to the equivalent circuit of a charge transfer resistance and a capacitor (CPE) connected in parallel. The larger figure shows the whole frequency range, where the impedance has bent towards the real axis, as the finite thickness of the cell begins to show in the lower frequencies, and approaches the value 620 Ω. To indicate the sensitivity of the fit towards the cell thickness, the dashed lines in Fig. 5a represent ± 5% changes in the cell thickness; roughly equivalent to ± 10% changes in $t_{D,R}$. The surface area shows similar sensitivity.

After fitting the isothermal measurement, the corresponding non-isothermal measurement was analyzed. The ohmic resistance was first determined and fixed. The surface area and the cell thickness were obtained from the isothermal measurement and it was assumed that their values remain unaffected by the applied temperature gradient. Again, the values for the CPE and R_{ct} were first obtained from the analysis of the high frequency data. Then, the Soret coefficient was the only fitting parameter in the analysis of the whole frequency range. The resulting fit for 10 mmol/L is shown in Fig. 5c as the solid line. The high frequency range is shown Fig. 5d. The two dashed curves in Fig. 5c correspond to ± 50% changes in the Soret coefficient. These curves evidence that the model is rather insensitive towards the Soret coefficient, and the uncertainty of the values calculated is at least 50%. This should be kept in mind when analyzing the results further.

Table 1 lists the best fit parameters of measurements in different concentrations: 50 mmol/L, 10 mmol/L, 5 mmol/L, and 1 mmol/L. The effective area is in very good agreement with the geometrical area. The diffusional time $t_{D,R}$ is also in very good agreement with its estimation based on the cell thickness and the diffusion coefficient at infinite dilution. The slight variations observed in $t_{D,R}$ could be related to the concentration dependence of the diffusion coefficient [22]. The ohmic resistance changes only slightly from one experiment to another. The electrode capacitance shows larger fluctuations.

The charge transfer resistance R_{ct} in Table 1 shows only small but aleatory changes between the isothermal and non-isothermal cases. The predicted effect of a temperature gradient to R_{ct} stems from two factors: the decrease in the electrode temperature, Eq. (17), and the decrease in the exchange current density due to the Soret effect, Eq. (14). A temperature difference of 10 K between the electrodes results in 5 K temperature decrease at the WE from the average temperature, ignoring the heat transfer losses. At 298 K this should result in a decrease of < 2% for R_{ct}. The impact of the Soret effect is more complicated to analyze thoroughly. If the Soret coefficients of the species are different, the analysis requires not only their values but also the charge transfer coefficients in Eq. (14). If their Soret coefficients are identical, as assumed in this study, the Soret effect slightly increases the exchange current density, which also decreases the charge transfer coefficient. However, the latter effect is likely to be even smaller than the former, and the variation observed here cannot be fully explained and has to be accepted as experimental error.

In the case of dilute solutions of simple monovalent electrolytes, the Soret coefficient has been reported to decrease linearly with increasing square root of the ionic strength $I = (1/2)\,\Sigma\, z_i^2 c_i$ [15]. With multivalent electrolytes and more concentrated solutions, the interactions between solvent and solute become more significant and complicated, and the dependence has been reported to deviate from linear behavior [3,12]. In the studied ionic strength range, the Soret coefficient is known to decrease with increasing ionic strength and our determinations of the apparent Soret coefficient of the ferro/ferricyanide ion are in agreement with both other experimental methods [12,15] and simulations [23]. Our results are also consistent (solid line in Fig. 6a) with the linear decrease with increasing $I^{1/2}$ arising from the influence of the Debye length on the dependence of the Soret coefficient [15]; note the 0.5 mol/L KCl supporting electrolyte. However, given the narrow range of ionic strength, a linear decrease with increasing I might also fit our results (dashed line in Fig. 6a). Since the Soret coefficient determined from impedance spectroscopy have significant uncertainty, as the experiments in the lowest ionic strength clearly show, further quantitative analysis at this point is otiose. The low precision stems from the fact that the Soret coefficient is usually small, and as it appears in the model inside an exponent, the sensitivity suffers. One strategy could be to apply a larger temperature difference, but a too high value would likely increase the convection near the electrodes.

Although the Soret coefficient is determined here with some uncertainty, its value is of the right order of magnitude. According to our results, the apparent Soret coefficient for the ferro/ferri redox-couple in the 1–10 mmol/L concentration region (in 0.5 mol/L KCl) is between 6×10^{-3} K^{-1} and 8×10^{-3} K^{-1}. This is in agreement with other studies in the literature: for $K_4Fe(CN)_6$ in 10 mmol/L (without

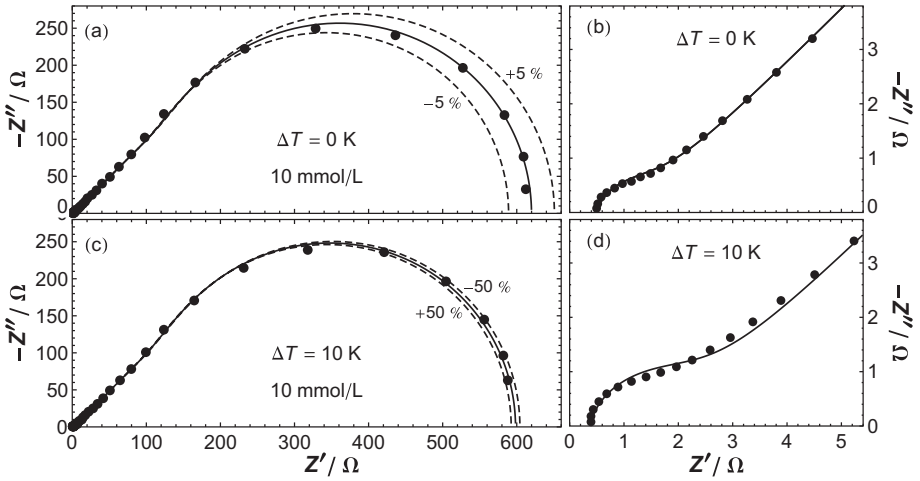

Fig. 5. EIS of 10 mmol/L $Fe(CN)_6^{4-}/Fe(CN)_6^{3-}$ in 0.5 mol/L KCl measured (f = 100 kHz − 1 mHz) at OCP and $\overline{T}$ = 298 K. The symbols represent experimental results and the solid line is the best fit to Eq. (17) with the parameter values shown in Table 1. Panel (a) shows the isothermal case and panel (c) a non-isothermal case with ΔT = 10 K. Panels (b) and (d) show the corresponding high frequency data fit. The dashed lines show how the fit changes: (a) when the cell thickness h is changed by ± 5%, and (c) when the Soret coefficient σ_T is changed by ± 50%.

Table 1
Best fit parameter values for different concentrations and temperature differences. In the isothermal measurements, A and $t_{D,R}$ were the only fitting parameters for the whole frequency range. In the non-isothermal measurements, σ_T was the only fitting parameter for the whole frequency range. In both cases, R_Ω, Q, n and R_{ct} were obtained from the analysis of the high frequency data.

c/mmol/L	ΔT/K	R_Ω/Ω	R_{ct}/Ω	Q/μF	n	A/cm^2	$t_{D,R}$/s	$10^3\sigma_T$/K^{-1}
50	0	0.54	0.47	2900	0.64	0.20	51.6	–
	10	0.53	0.48	1800	0.67			1.8
10	0	0.50	1.1	70	0.87	0.20	49.5	–
	10	0.37	2.0	69	0.87			6.0
5.0	0	0.50	3.2	71	0.83	0.26	50.8	–
	10	0.45	2.8	62	0.85			6.6
1.0	0	0.60	66	54	0.84	0.19	56.2	–
	10	0.70	71	100	0.78			4.2
	10	0.73	110	68	0.82			7.1
	20	0.57	77	150	0.72			9.1

supporting electrolyte) the Soret coefficient has been reported as 5.2×10^{-3} K^{-1} [13] and in 2 mol/L KCl supporting electrolyte as 5×10^{-3} K^{-1} − 10×10^{-3} K^{-1} in 50 mmol/L [2]. With the literature lacking more extensive data on the concentration dependence of the Soret coefficient and the effect of the supporting electrolyte, a comprehensive analysis on the validity is impossible.

The effective surface area remains very close to the geometrical surface area of 0.196 cm^2 in all the experiments (Table 1). The cell thickness varies very little from one experiment to another, indicating that the cell assembly (tightening of the screws) contributed only little to its experimental variation. The dispersion of the values of these parameters can be graphically assessed by calculating the ohmic resistance associated with species i, Eq. (17). For the oxidized species, $R^s_{O,eq} = RT(0)h/(2F^2AD_O c^b_{O,eq}E_{\theta,O})$ should be a linear function of the reciprocal surface concentration at equilibrium, and Fig. 6b indeed shows a reasonable linear trend.

5. Conclusions

Although the Soret effect affects both the mass transport and the reaction kinetics, the latter effect was found to be negligible. Therefore, the study focused on the mass transport effects of thermodiffusion. The mass transport in a thin-layer cell is visible in the Nyquist-plot as a low-frequency semicircle, with the curve bending towards the real axis at low frequencies. In isothermal conditions, it is a function of the thickness of the cell, the concentrations of the reacting species, and their diffusion coefficients. When a temperature gradient is imposed to the cell, the temperature difference of the two electrodes, and the Soret coefficient appear as additional parameters in the model. In the case of a positive temperature difference (WE is colder than the CE) and a positive Soret coefficient (thermophobic behavior), the Soret effect decreases the diameter of the semicircle, i.e. enhances the mass transport towards the WE. Should the Soret coefficient be negative, the size of the semicircle would increase. Here, the former case was experimentally verified.

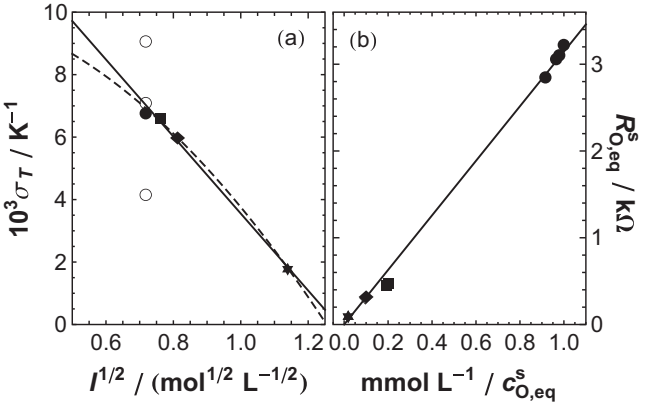

Fig. 6. (a) The Soret coefficient of the reacting species decreases with increasing ionic strength. The symbols represent measurements in different concentrations of the ferro/ferri couple: 50 mmol/L (triangle), 10 mmol/L (diamond), 5 mmol/L (square), 1 mmol/L (open circles are different measurements and filled circle is their average); note the 0.5 mol/L KCl supporting electrolyte. The solid line shows the best fit for a linear decrease with increasing square root of the ionic strength, in agreement with the theoretical predictions and experimental observations in Ref. [15]. Our results, however, are not conclusive as to the dependence on I. The dashed line shows the best fit for a linear decrease with increasing I, which could also be consistent with our results. (b) The resistance associated with the oxidized species, $R^s_{O,eq} = RT(0)h/(2F^2AD_O c_O{}^b E_{\theta,O})$, calculated with the parameters in Table 1 and the diffusion coefficient corresponding to infinite dilution at 298 K. The resistance increases linearly with the reciprocal surface concentration in Soret equilibrium.

The simulations showed that although the Soret effect is clearly visible in the impedance spectrum, this spectrum is very sensitive to the diffusional times $t_{D,i} = h^2/4D_i$. Therefore, these times need to be precisely known before determining the Soret coefficients from the experiments. Here, the problem was addressed by fixing the ratio D_R/D_O of the diffusion coefficients to its value at infinite dilution, and determining $t_{D,R}$ from isothermal measurements.

Previous research into the thermodiffusion of the ferro/ferricyanide redox-couple in KCl supporting electrolyte suggests that their Soret coefficients might be different [2] (the author estimated a relatively small difference of 2×10^{-3} K^{-1}). Our simulations, however, suggested that observing the difference of the Soret coefficients of the different species is by no means straightforward using EIS. As one species having a slightly different Soret coefficient changed the impedance spectrum only slightly, studying their relative differences with accuracy in the present experimental conditions would be difficult. As suggested at the end of Section 2, it could be possible to estimate this with experiments at different concentration ratios of the reduced and oxidized species, and to verify the reported difference. However, such experiments were deemed outside the scope of the study. The Soret coefficient was determined in different concentrations and the results confirmed that the coefficient decreases with increasing ionic strength, which agrees with the observations made using other experimental techniques as well as MD simulations [12,15,23]. Moreover, within the studied concentration range, our results are consistent with a linear dependence of the square root of the ionic strength, as predicted theoretically in dilute solutions [15]. However, as the range is relatively narrow, they are also consistent with, e.g., a linear decrease of the Soret coefficient with increasing ionic strength, and should be considered inconclusive as far as the exact dependence on the ionic strength is concerned. Because the values obtained here have a significant uncertainty, future efforts should be focused on improving the setup and increasing the reproducibility of the results. Several strategies could be pursued, e.g. decreasing further the cell thickness and decreasing the surface area of the electrode. Nevertheless, we have successfully shown that the Soret coefficient of a trace ion can be determined using impedance spectroscopy and have obtained results in agreement with literature data.

Acknowledgements

M. J. wishes to thank Aalto Energy Efficiency Research Programme (Heat-Harvest), the School of Chemical Engineering at Aalto University, and the Kaute foundation, for financial support. J. A. M. acknowledges the support from European Regional Development Funds and the Ministerio de Economía y Competitividad through project MAT2015-65011-P. Mr. Heikki Viianranta is gratefully acknowledged for helping with the design and constructing the measurement cell. Mr. Tuomas Vainikka and Dr. David Lloyd are thanked for their helpful input and discussions regarding the experimental setup.

Appendix A. Supplementary data

Supplementary data to this article can be found online at https://doi.org/10.1016/j.jelechem.2018.04.054.

References

[1] S.R. de Groot, P. Mazur, Non-Equilibrium Thermodynamics, North-Holland Publishing Co., Amsterdam, 1962.
[2] A. Boika, Mass Transport Phenomena at Hot Microelectrodes, PhD Thesis University of Saskatchewan, Saskatoon, 2010.
[3] M. Jokinen, J.A. Manzanares, K. Kontturi, L. Murtomäki, Thermal potential of ion-exchange membranes and its application to thermoelectric power generation, J. Membr. Sci. 499 (2016) 234.
[4] C.J. Petit, M. Hwang, J. Lin, Thermal diffusion of dilute aqueous NH_4Cl, Me_4NCl, Et_4NCl, n-Pr_4NCl, and n-Bu_4NCl solutions at 25 °C, J. Solut. Chem. 17 (1988) 1.
[5] P. Reineck, C.J. Wienken, D. Braun, Thermophoresis of single stranded DNA, Electrophoresis 31 (2010) 279.
[6] K. Maeda, N. Shinyashiki, S. Yagihara, S. Wiegand, R. Kita, Ludwig-Soret effect of aqueous solutions of ethylene glycol oligomers, crown ethers, and glycerol: temperature, molecular weight, and hydrogen bond effect, J. Chem. Phys. 143 (2015) 124504.
[7] Y. Kishikawa, S. Wiegand, R. Kita, Temperature dependence of Soret coefficient in aqueous and nonaqueous solutions of pullulan, Biomacromolecules 11 (2010) 740.
[8] D.G. Leaist, L. Hao, Very large thermal separations for polyelectrolytes in salt solutions, J. Chem. Soc. Faraday Trans. 90 (1994) 1909.
[9] M. Kreysing, L. Keil, S. Lanzmich, D. Braun, Heat flux across an open pore enables the continuous replication and selection of oligonucleotides towards increasing length, Nat. Chem. 7 (2015) 203.
[10] L.G. Longsworth, The concentration and temperature dependence of the Soret coefficient of some aqueous electrolytes, in: W.J. Hamer (Ed.), The Structure of Electrolyte Solutions, John Wiley & Sons, Inc., New York, 1959, p. 183.
[11] S. Wiegand, H. Ning, H. Kriegs, Thermal diffusion forced Rayleigh scattering setup optimized for aqueous mixtures, J. Phys. Chem. B 111 (2007) 14169.
[12] P.N. Snowdon, J.C.R. Turner, The concentration dependence of the Soret effect, Trans. Faraday Soc. 56 (1960) 1812.
[13] P.N. Snowdon, J.C.R. Turner, The Soret effect in some 0.01 normal aqueous electrolytes, Trans. Faraday Soc. 56 (1960) 1409.
[14] J.N. Agar, J.C.R. Turner, Thermal diffusion in solutions of electrolytes, Proc. Royal. Soc. A 255 (1960) 307.
[15] J.N. Agar, Thermal diffusion and related effects in solutions of electrolytes, in: W.J. Hamer (Ed.), The Structure of Electrolyte Solutions, John Wiley & Sons, Inc., New York, 1959, p. 200.
[16] Z.A. Rotenberg, Thermoelectrochemical impedance, Electrochim. Acta 42 (1997) 793.
[17] R. Haase, Thermodynamics of Irreversible Processes, Dover, Mineola, N.Y, 1990.
[18] O. Contamin, E. Levart, D. Schuhmann, Étude de l'impédance de concentration sur une cellule à couche mince, J. Electroanal. Chem. Interfacial Electrochem. 84 (1977) 287.
[19] D.R. Lide, CRC Handbook of Chemistry and Physics, 75th edition, CRC Press, Inc., Boca Raton, Fla., 1994.
[20] J.L. Dellis, Matlab function, MATLAB Central File Exchange, https://se.mathworks.com/matlabcentral/fileexchange/19460-zfit, (2010) (Zfit version 1.2 Retrieved April 18, 2016).
[21] R. Mills, V.M.M. Lobo, Self-diffusion in electrolyte solutions a critical examination of data compiled from the literature, Physical Sciences Data, Vol. 36 Elsevier Science Publishers B.V, Amsterdam, 1989.
[22] S.A. Mareev, D.Yu. Butylskii, A.V. Kovalenko, A.V. Petukhova, N.D. Pismenskaya, L. Dammak, C. Larchet, V.V. Nikonenko, Accounting for the concentration dependence of electrolyte diffusion coefficient in the Sand and the Peers equations, Electrochim. Acta 195 (2016) 85.
[23] S.D. Lecce, T. Albrecht, F. Bresme, The role of ion-water interactions in determining the Soret coefficient of LiCl aqueous solutions, Phys. Chem. Chem. Phys. 19 (2017) 9575.

Supporting Information

Soret Coefficient of Trace Ions Determined with Electrochemical Impedance Spectroscopy in a Thin Cell. Theory and Measurement

Miikka Jokinen[1], José A. Manzanares[1,2], Lasse Murtomäki*,[1]

[1] Department of Chemistry, School of Chemical Engineering, Aalto University, P.O. Box 16100, FI-00076 Aalto, Finland

[2] Department of Thermodynamics, Faculty of Physics, University of Valencia, E-46100 Burjassot, Spain

* Corresponding author. E-mail: lasse.murtomaki@aalto.fi

Compared to the Nyquist plots used in the main text, the Bode plots presented in this Supporting Information file show more clearly the impedance information in the frequency domain. Thus, the frequency regions where different parameters, associated to different electrochemical processes, are relevant may become clearer. Figure SI.1 shows the simulation results for the effect of the cell thickness in the impedance. Actually, the impedance is very sensitive to the diffusion time, which combines the cell thickness and the ionic diffusion coefficients, but concentrating on the cell thickness h helps in understanding the key role of mass transport in a confined space (an electrochemical thin cell) on the impedance.

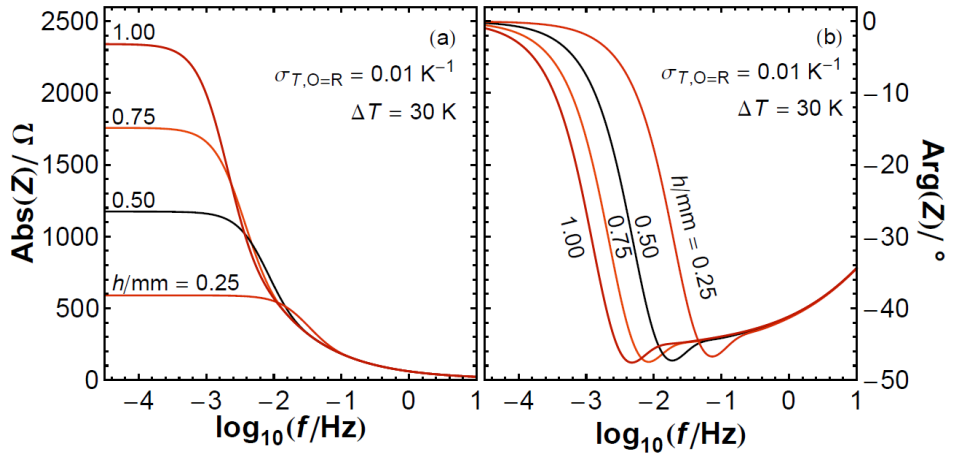

Figure SI.1. The Bode plots of the simulated thermodiffusion impedance clearly illustrate the effect of the cell thickness h on the spectrum. These simulations correspond to bulk concentrations $c_O^b = c_R^b = 5$ mmol/L, electrode diameter $d = 5$ mm, $\bar{T} = 298$ K, $R_\Omega = 1\,\Omega$, $C_{dl} = 5\,\mu$F, $R_{ct} = 5\,\Omega$, and $D_O = D_R = 10^{-5}$cm^2/s. The color code is the same as in Fig. 3c of the main text. The frequency range considered here has been chosen to clearly illustrate the effect of the cell thickness and it does not correspond to the frequency range analyzed in the experiments.

Figure SI.2 shows the Bode plots of the experimental results for $c_{\mathrm{O}}^{\mathrm{b}} = c_{\mathrm{R}}^{\mathrm{b}} = 10$ mmol/L, both for the isothermal measurements and for the measurements with a temperature gradient. The circles represent the experimental points and the lines are fit results. See the discussion of Fig. 5 in the main text for further details.

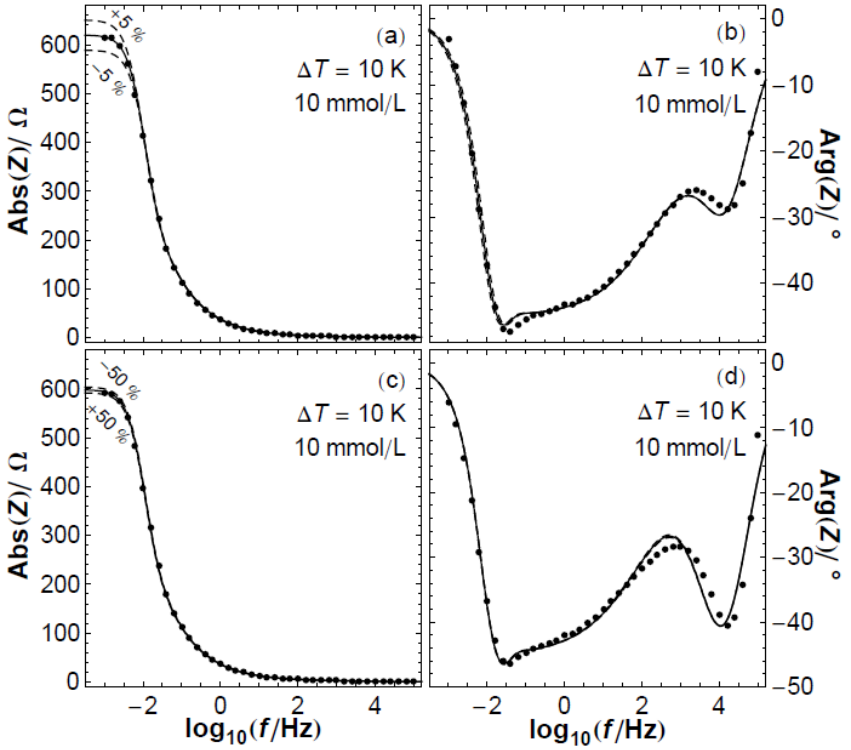

Figure SI.2. Bode plots of the measured EIS of 10 mmol/L $\mathrm{Fe(CN)_6^{4-}/Fe(CN)_6^{3-}}$ in 0.5 mol/L KCl measured ($f = 100$ kHz – 1 mHz) at OCP and $\bar{T} = 298$ K. The symbols represent experimental results and the solid line is the best fit to eq. (20) with the parameter values shown in Table 1. Panels (a) and (b) show the magnitude and argument of the complex impedance in the isothermal case. Panels (c) and (d) show the magnitude and argument of the complex impedance in the non-isothermal case ($\Delta T = 10$ K). The dashed curves show how the fit changes: (a) and (b) when the cell thickness h is changed by ±5 %, and (c) and (d) when the Soret coefficient σ_T is changed by ±50 %; the dashed curves practically overlap with the solid curves in the plots of the argument of the impedance.